GA–A25253

THE GENERAL ATOMICS FUSION THEORY PROGRAM ANNUAL REPORT FOR GRANT YEAR 2005

by
PROJECT STAFF

OCTOBER 2005

GENERAL ATOMICS

DISCLAIMER

GA–A25253

THE GENERAL ATOMICS FUSION THEORY PROGRAM ANNUAL REPORT FOR GRANT YEAR 2005

by
PROJECT STAFF

Work supported by
the U.S. Department of Energy
under Grant No. DE-FG03-95ER54309

GENERAL ATOMICS PROJECT 03726
OCTOBER 2005

GENERAL ATOMICS

ABSTRACT

The dual objective of the fusion theory program at General Atomics (GA) is to significantly advance our scientific understanding of the physics of fusion plasmas and to support the DIII–D and other tokamak experiments. The program plan is aimed at contributing significantly to the Fusion Energy Science and the Tokamak Concept Improvement goals of the Office of Fusion Energy Sciences (OFES).

1. HIGHLIGHTS OF THEORY WORK IN GY05

During the past year, considerable progress was made in each of the important areas of our research program:

- The basic building blocks for an advanced gyro-fluid transport model to replace GLF23 are in place. These include a new system of trapped gyro-Landau fluid (TGLF) equations that are being generalized to finite β and real geometry and are valid over a much broader parameter range, creation of a database of over 300 nonlinear GYRO simulations for benchmarking, and theoretical understanding of non-local transport.
- Various novel turbulence studies were completed with the GYRO code, and further improvements to the core solver were incorporated. Notably, the capability now exists to simulate higk-k ETG turbulence rigorously coupled to low-k ITG/TEM turbulence. This capability includes an FFT-based nonlinear discretization scheme to complement the older direct scheme.
- A general drift-kinetic equation with rotation has been derived without assuming the flow velocity is small or specializing its form.
- A new calculation of neoclassical angular momentum flux with small rotation is completed that results in a significant correction to a 34-year old result. The calculation relies on recent large-aspect-ratio perturbative results on distribution functions that bypass the need to solve a second-order drift kinetic equation.
- A globally convergent Newton method based module GCNM for solution of stiff transport equations was developed as part of the US Integrated Fusion Modeling efforts. The module provides an efficient tool to analyze plasma transport with a stiff transport model such as GLF23.
- A 116 processor (64-bit AMD Opteron) Linux cluster with Infiniband interconnect is fully operational. GYRO, ORBIT-RF, and NIMROD have been ported to the new cluster and are running in production mode.
- The ELITE edge stability code was improved and applied to further validate the peeling-ballooning model for Edge Localized Modes (ELMs). This includes testing of the model against DIII-D quiescent H-mode discharges without ELM and I-coil ELM suppression discharges, and comparison of predicted filamentary structure against observed light emission during ELMs.
- Simulations of ELM onset and evolution were continued in a coordinated effort using BOUT and NIMROD to describe the nonlinear physics of ELMs. This includes extensive NIMROD calculations with realistic DIII-D profiles and shape

as part of a 2005 DoE Theory milestone on ELM simulations. This effort has advanced our understanding of the transfer of energy between modes via nonlinear coupling, and the effects of dissipation, in ELMs.

- Modeling of feedback stabilization with MARS-F has verified the importance of phasing angle in the stabilization of resistive wall modes (RWM) as observed in DIII-D.
- In collaboration with scientists at National Institute for Fusion Science in Japan (NIFS), a method has been formulated to compute the growth rate of a weakly unstable resistive wall mode (RWM) in 3D configurations using results from ideal stability codes.
- Ideal stability study of configurations with double transport barriers suggests that modest edge transport barriers (ETB) can improve plasma stability, but strong ETBs can drive ideal MHD instabilities with a substantial edge component.
- The improved Monte-Carlo code ORBIT-RF coupled with the TORIC4 full wave code was successfully applied to model C-Mod and DIII-D ICRF experiments. ORBIT-RF and TORIC4 results agree with the experimentally measured C-Mod fast ion energy spectrum and weak wave-particle interactions in DIII-D when 116 MHz (8th harmonic) FW was applied to beam-heated discharges.
- Fuel deposition profiles using the recently improved pellet ablation model with allowance for arbitrary pellet poloidal entry angle agree well with the DIII-D inside and outside launch pellet data.

As a consequence of these results, scientists from the Theory Group were selected to give a number of invited talks and colloquia as highlighted in the next section. Following this are more detailed descriptions of the advances and achievements made in each of the major areas.

2. SIGNIFICANT PRESENTATIONS IN GY05

- J.E. Kinsey presented "Transport Modeling and Gyrokinetic Analysis of Advanced High Performance Discharges," at the 20th IAEA Fusion Energy Conference in Vilamoura, Portugal, November 1-6, 2004.
- P.B. Parks presented "Recent Advances in the Theory and Simulation of Pellet Ablation and fast Fuel Relocation in Tokamaks," at the 20th IAEA Fusion Energy Conference in Vilamoura, Portugal, November 1-6, 2004.
- R.E. Waltz gave an oral presentation "Advances in Comprehensive Gyrokinetic Simulations of Transport in Tokamaks," at the 20th IAEA Fusion Energy Conference in Vilamoura, Portugal, November 1-6, 2004.
- P.B. Snyder presented an invited talk on "Toroidal Rotation and 3D Nonlinear Dynamics in the Peeling-Ballooning Model of ELMs" at the 2004 APS Meeting in Savannah, GA, November 15-19, 2004.
- R.E. Waltz gave an invited presentation "Gyrokinetic Simulations and Multi-scale Processes," at the UCLA-PAM Workshop on "Multi-scale Processes in Fusion Plasmas" in Los Angeles, CA, Jan 10-14, 2005.
- M. Choi gave an invited presentation "Monte-Carlo Orbit/Full-Wave Simulation of Fast Alfven Wave Damping on Resonant Ions in Tokamaks," at the 16th Topical Conference on Radio Frequency Power in Plasmas in Park City, Utah, April 11-13, 2005.
- D. Brennan and C. Estrada-Mila presented oral talks on "Nonlinear Evolution of Edge Localized Modes" and "Gyro-kinetic Simulations of Ion and Impurity Transport" at the 2005 International Sherwood Fusion Theory Conference in Stateline, Nevada, April 11-13, 2005.
- J. Candy presented an oral talk on "History of GYRO Verification and Suggestions for Future Development Practices" at the 9th Joint US-European TTF Workshop in Napa, California, April 6-9, 2005.
- P.B. Snyder presented a talk on "Dual Transport Mechanisms for ELMs" at the 9th Joint US-European TTF Workshop in Napa, California, April 6-9, 2005.
- J. Candy presented an oral talk on "The General Atomics DROP Cluster" at the 2005 International Sherwood Fusion Theory Conference in Stateline, Nevada, April 11-13, 2005.
- J. Candy gave an oral presentation "GYRO Performance on MPP Systems" at the 2005 Cray User Group (CUG) Meeting in Albuquerque, NM, May 16-19, 2005.

- V.S. Chan gave a presentation "Simulation of Fast Alfvén Wave Interactions with Neutral-Beam and Minority Ions in Tokamaks" at the 32nd EPS Plasma Physics Conference in Tarragona, Spain, June 27 – July 1, 2005.
- P.B. Snyder gave an oral presentation "Nonlinear Dynamics and Energy Loss Mechanisms of ELMs" at the 32nd EPS Plasma Physics Conference in Tarragona, Spain, June 27 – July 1, 2005.
- V.S. Chan gave an oral talk on "Simulation of ICRF Interactions with Fast Ions and Modification of MHD Stability" at the US-Japan JIFT Workshop on Integrated Modeling of Multi-scale Physics in Fusion Plasmas in Kyushu, Japan, September 13-15, 2005.

3. ADVANCES IN TRANSPORT RESEARCH

3.1. GYRO DEVELOPMENT AND APPLICATIONS

With relatively minor modifications to the existing GYRO solver, we can now simulate short-scale ETG turbulence rigorously embedded in long-wavelength ITG-TEM turbulence. These simulations have a very high equivalent Reynolds number and require enormous computational resources. To this end, an alternative FFT algorithm for evaluating the Poisson bracket nonlinearity has also been developed and coded. GYRO can switch to this method at the largest problem sizes for maximum efficiency. For low-k ITG/TEM modes, we have verified that the new electron treatment, which retains electron gyro-radius effects non-perturbatively, closely reproduces the older (faster) perturbative method. Given adequate resources, we plan to carry out simulations that fully couple nonlinear ETG effects to the usual ITG-TEM turbulence.

Equations that describe the evolution of volume-averaged entropy were derived and added to GYRO. In particular, the creation of entropy through spatial upwind dissipation (there is zero velocity-space dissipation in GYRO) and the reduction of entropy via the production of fluctuations can be monitored. This new diagnostic has yielded several key confirmations of the validity of the GYRO simulations. First, fluctuations balance dissipation in the ensemble-averaged sense, thus demonstrating that turbulent GYRO simulations achieve a true statistical steady state. Second, at the standard spatial grid size, neither entropy nor energy flux is significantly changed by a sixteen-fold increase in velocity-space resolution. Third, the measured flux is invariant to an eight-fold increase in the upwind dissipation coefficients. Thus, the lack of change in entropy with grid refinement refutes the familiar but incorrect notion that Eulerian gyro-kinetic codes miss important velocity-space structure.

Work on the β scaling of transport coefficients in gyro-kinetic micro-turbulence simulations was completed and published. Various unanticipated results were obtained. First, it proved to be extremely difficult to run GYRO at greater than half the (local) MHD critical β. This is perhaps the result of magnetic island formation in the vicinity of rational surfaces, where electrons are strongly resonant. Indeed, modifications of the electron temperature gradient are most pronounced at rational surfaces (Fig. 1). As β was increased from zero, the electron energy transport (χ_e) acquires a pronounced electromagnetic (flutter) component. Indeed, half of χ_e is due to magnetic flutter at $\beta/\beta_{crit} = 0.6$. The ion energy transport (χ_i), in the other hand, remains purely electrostatic and is only weakly affected by β.

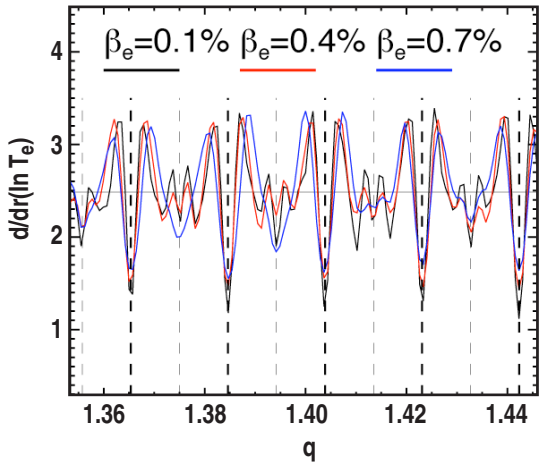

Fig. 1 Electron temperature fluctuations as computed by nonlinear GYRO simulations of electromagnetic turbulence. Thick (thin) vertical dashed lines indicate first-order (second-order) rational surfaces.

The stabilizing effect of *E×B* shear on turbulence was also studied using GYRO. It was found that the *E×B* shear quench rule, originally deduced from ITG simulations with adiabatic electrons (ITG-ae), also applies in the presence of kinetic electrons. The quench point is amazingly robust at $\gamma_E/\gamma_{max} = 2$ (+/- 0.5) for both adiabatic and kinetic electron cases examined. This quench point is twice the value found in nonlinear gyro-fluid simulations. In kinetic electron simulations of peaked density cases, where the unstable modes are primarily in the electron direction, the *E×B* shear quench point occurs at somewhat higher values in the range of $\gamma_E/\gamma_{max} = 2.3$ (+/- 0.2).

Simple ITG-ae simulations have also been done to quantify the non-local transport mechanism for breaking gyro-Bohm scaling. The simulations are described by a heuristic formula for a non-local growth rate (a weighted average of nearby local growth rates) that can be used in place of the local growth rate in transport models like GLF23. This will quantify, as a function of ρ* and growth rate, how turbulence from (locally) unstable regions drains into (locally) stable regions. Gyro-Bohm transport scaling will be broken toward Bohm in the unstable regions and toward super gyro-Bohm scaling in the stable (or less unstable) regions.

The first GYRO simulations of DIII-D H-modes track the slightly super gyro-Bohm experimental scaling of the ρ* pair, which have about 1.5 times larger ρ* than the well-studied L-mode pair. Compared with the L-mode pair, the H-mode pair has normalized growth rates half as large and weaker *E×B* shear. The large *E×B* shear in the L-mode pair (even though it is ρ* invariant) may be driving the system closer to threshold, where Bohm scaling is more easily achieved. A perfect rescaling of the small ρ* L-mode experimental profile data to the larger ρ* gives perfect Bohm scaling in simulations. However, a perfect rescaling of the small ρ* H-mode to the larger ρ* is close to Bohm scaling, suggesting the

near gyro-Bohm scaling observed in H-mode experiments is due to experimental imperfections in profile similarity.

An extensive series of GYRO simulations, variants of a standard (STD) test case, have been performed to create a gyro-kinetic transport database. For simplicity, the simulations are electrostatic and consider only local effects. Variations of safety factor, magnetic shear $\hat{s}$, MHD α parameter, $E\times B$ shear, etc. have been treated. Both ITG and TEM-dominated regimes have been considered. The database of more than 300 nonlinear simulations will be used for benchmarking and to fit and test the new TGLF transport model that is currently under development. A sample scan is reproduced in Fig. 2. Here, variation of the magnetic shear shows the transition from a (collisionless) particle pinch to outward flow at $\hat{s} = 0.5$.

GYRO simulations of ETG modes with adiabatic ions have been used to supplement the theoretical work on discrete particle noise by Nevins and Hammett. A computationally "easy" benchmark case for which ETG turbulence saturates at a low level was found through various GYRO simulations. An inter-code benchmark with Dimits' PIC code (PG3EQ) on this low-transport case was very successful. Moving to more unstable cases showed a dramatic difference in turbulence levels, which could be successfully explained by discrete particle noise in the PIC simulations.

Recent GYRO work has been focused on studying the effects of elongation κ and triangularity δ in simulations including kinetic electrons. Scans in κ around the STD case revealed that the GYRO diffusivities robustly follow an inverse linear dependence on κ. This result appears to be valid over a wide range of safety factor q and magnetic shear values. This result appears to differ from previous gyro-fluid ITG simulations that showed a κ dependence varied with q. Converting the GYRO diffusivities to the ITER definition we find that χ scales as $\kappa^{-2.3}$ which may be significant.

As previously reported, the parallel Ohmic heating is related to the parallel nonlinearity (PNL), a small effect normally ignored in gyro-kinetic simulations (formally, one order in $\rho*$ smaller than the standard terms). We have carried out new GYRO simulations (local runs with ITG-ae physics) including the PNL and, as expected, see no significant effect on energy transport for $\rho* < 1.5\%$. We were careful to remove secular effects that correspond to the turbulent heating in the transport equation. We believe recent reports of significant effects from the PNL (W.W. Lee, invited talk, APS 2004) in global PIC codes are erroneous, perhaps due to discrete particle noise (as described by the recent Nevins-Hammett theory) or spurious profile relaxation in global codes.

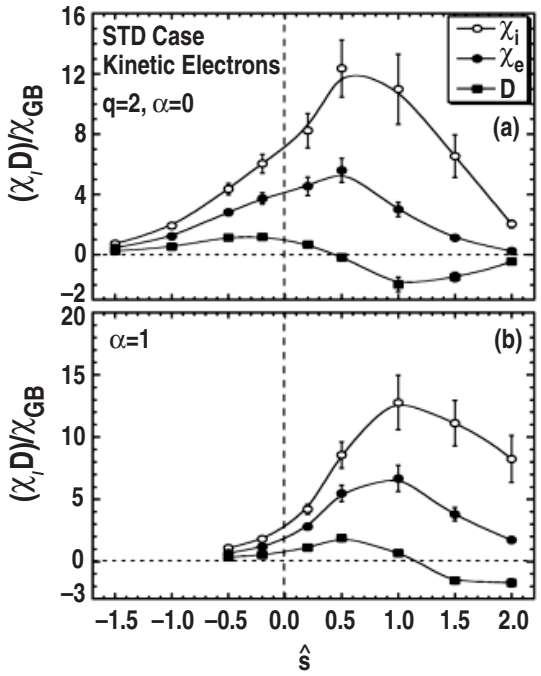

Fig. 2 Time-averaged ion and electron energy diffusivity and particle diffusivity versus magnetic shear for (a) $\alpha = 0$ and (b) $\alpha = 1$ from GYRO nonlinear simulations with kinetic electrons around the standard case.

3.2. GLF23 TRANSPORT MODEL DEVELOPMENT

A new system of gyro-Landau fluid (GLF) equations has been finalized for the new GLF23 model. The new trapped gyro-Landau fluid (TGLF) model equations include trapped particles in a more accurate way and are being generalized to include real geometry and finite β. The model yields excellent fits to GKS linear eigenmodes continuously from low-k trapped ion modes to intermediate-k TEM modes to high-k ETG modes. The model was extensively benchmarked against a large GKS linear stability database comprised of 1799 GKS runs with systematic scans around the standard, NCS, and H-mode pedestal reference cases (Fig. 3). The growth rates agree within 11.4% over the whole database and the average deviation of the total eigenvalue is 18.0%. The new TGLF model agrees significantly better with the GKS results than the original GLF23 model. The new set of gyro-fluid equations has been named TGLF for trapped gyro-Landau Fluid and a paper on the model will be published in the October issue of Physics of Plasmas. The main improvements over previous GLF models are:

- A model for the loss of averaging of the Landau resonance by trapped particles that makes the model valid for all frequencies.
- High accuracy finite Lamor radius integrals that include the impact of the trapped passing boundary and are valid for all aspect ratios, trapped fractions, and perpendicular wave numbers.

- Splitting of the circulating particle moments into two pieces to give a much more accurate model of the two different frequency scales in the circulating particle response.
- Closure coefficients for the toroidal drift terms that include finite Lamor radius corrections.
- An adaptive Hermite basis function solution technique to obtain good accuracy with a small number of ballooning angle moments.

Work has begun on the numerical implementation of various physics modules for the new TGLF model. The shaped magnetic geometry subroutines have been written (adapted from the GYRO versions) and tested. These routines were written in such a way that they can use either input from an actual equilibrium with the Mercier-Luc local expansion or Miller geometry can be used in the absence of an equilibrium solution. The plan is to adapt the subroutines used in the ELITE code that computes various needed components of the magnetic fields on a flux surface contour. A model for electron-ion collision has also been derived and is being tested in the code. The next step will be to add electromagnetic fluctuations. These additions will give the new TGLF model complete gyro-kinetic physics except for rotation.

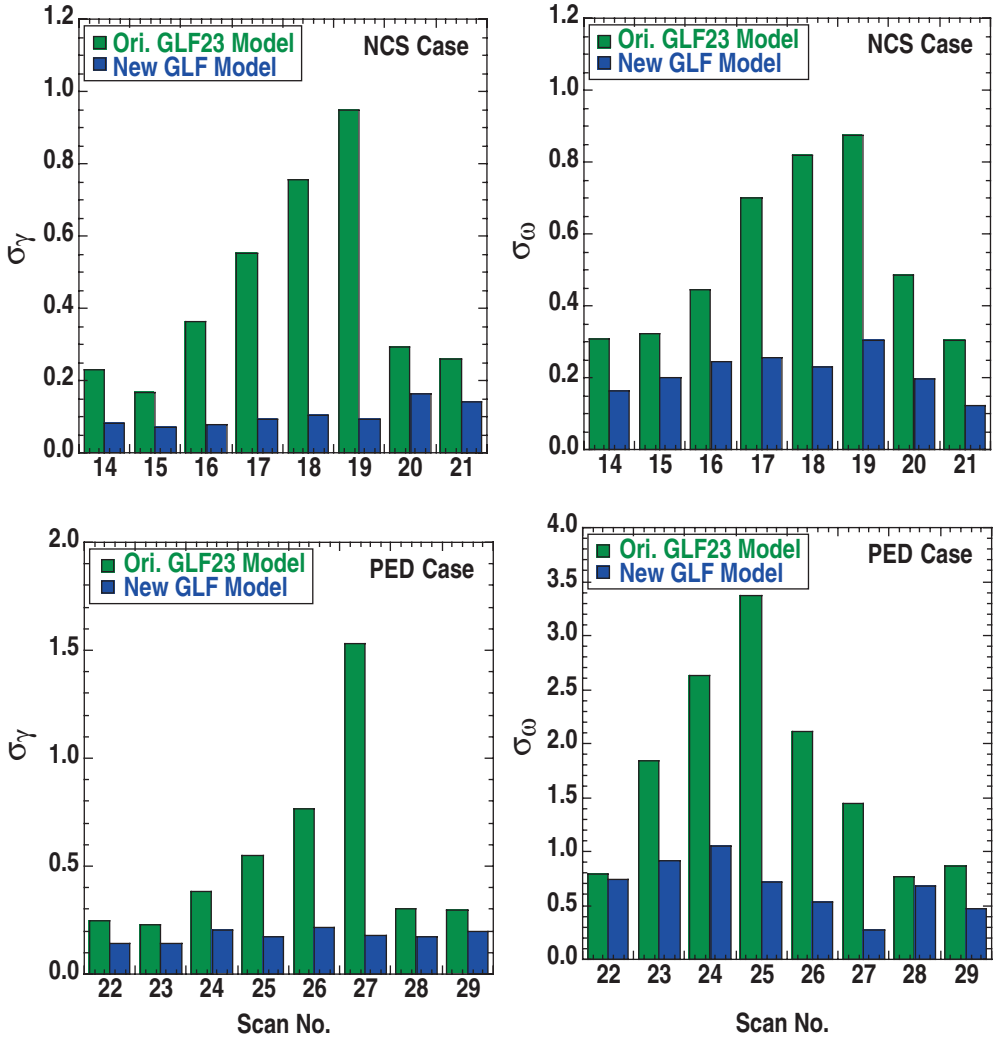

Fig. 3 Comparison of the growth rates and frequency from a 4 basis-function version of the new GLF23 model and the original GLF23 model against the GKS results.

3.3. TRANSPORT CODE MODULE DEVELOPMENT

A globally convergent Newton method based module, GCNM, for solution of stiff transport equations typically encountered in the analysis and modeling of DIII-D and other tokamaks was developed. This module will be part of the NTCC "Predictive TRANSP" project and is also included in the SWIM project. The module demonstrates the setup of some of the transport equations required to use the solver, analytic and numerical test cases and use of GLF23. It was created to allow easy addition of MPI and OpenMP parallel methods in the near future. The methods developed are suitable for "small scale" problems where direct (as opposed to iterative) solvers are suitable. However, extension to large sparse systems can be done if, for example, it is found that a more direct coupling between core and edge models is appropriate.

3.4. TRANSPORT THEORY DEVELOPMENT

General expressions for turbulent heating were derived, which are consistent with the drift-kinetic or gyro-kinetic approximations for the turbulent fluctuations. The mean distribution function is the solution of a drift-kinetic equation that is the Hazeltine (1973) equation with additional terms containing the turbulent fluctuations. Using as independent variables the parallel velocity and magnetic moment of a particle, Liouville's theorem is satisfied, so the equation can be written exactly in conservative form. The energy flux and heating rate were identified from the energy moment of the mean drift-kinetic equation. Both neoclassical and turbulent terms are included. The turbulent heating terms include the energy moment of the parallel nonlinearity, which is essentially the turbulent ohmic heating. Additional turbulent heating terms depending on finite gyro-radius are also obtained. The compete set of turbulent heating terms will be added to GYRO and evaluated. The radially integrated heating is expected to offset about 5-10% of the turbulently transported power.

The effects of electron-ion collisions on the linear zonal flow polarization have also been clarified. Including the m=0, +1, -1 potentials, it is found that the "dispersion relation" for the zonal flows has a damped root at approximately the electron-ion collision frequency, but the residual is approximately unaffected. That is, the response function for times much larger than a collision time (the residual) differs from the response function for times much smaller than a collision time by a small amount, proportional to the fraction of trapped electrons. The residual differs from the collisionless residual, obtained previously including only the m=0 potential, only by terms higher order in ion Larmor radius than previously kept. The reason for the small effect of electron-ion collisions is that the electrons only respond to the m= +1, -1 potentials, which are smaller than the m=0 potential by two orders in the ion Larmor radius.

A general drift-kinetic equation with rotation has been derived without assuming the flow velocity is small or specializing its form. The kinetic energy and magnetic moment of particles are defined in a frame moving with the flow, and they are not constant but change with time in a way that depends on details about the flow. We are attempting to simplify the results using a particular form for the flow, corresponding to sheared toroidal rotation.

The calculation of angular momentum flux in the small rotation version of neoclassical theory of transport is completed, resulting in a significant correction to a 34-year old result that involves a sign change. The result can be used to predict steady-state toroidal rotation profiles for discharges with no momentum source using density, temperature, and q profiles. The calculation relies on recent large-aspect-ratio perturbative results on distribution functions.

A work to include impurity ions in neo-classical flows with finite orbit was started in collaboration with W.X. Wang of PPPL. The goal is to be able to use measurements of impurity flows to determine the main ion flows and the radial electric field using Wang's δf

particle code. Although the NCLASS code can compute these, it uses many approximations. Thus, a first principle calculation is needed, especially when orbit widths may not be small compared with gradient lengths. As a first step, various model collision operators have been generalized to include two ion species.

3.5. LINUX PARALLEL CLUSTER

A new $300K Linux cluster, designed for use by the GYRO and NIMROD codes, was installed. The base configuration is completed and the system performance exceeds expectations. The cluster is logically partitioned into a set of three high performance sub-clusters, which communicate over an Infiniband network. The entire system is remotely manageable over a serial console. The system exports a RAID5 file system over NFS via gigabit Ethernet.

4. ADVANCES IN MHD STABILITY RESEARCH

4.1. EDGE STABILITY AND ELM ONSET

The ELITE code has been modified to allow stability studies of toroidal mode numbers (*n*) as high as 1000, and is the first MHD stability code to be successfully quantitatively benchmarked for both low to intermediate and very high toroidal mode numbers with GATO and BALMSC. These high-*n* studies with ELITE have shown that, for typical H-mode equilibria, the infinite-*n* ballooning limit is generally not quantitatively reached until *n* becomes very large (of order 10^2 - 10^3). These large *n* values typically exceed the physical finite-Larmor radius cutoff which occurs for $k_\theta \rho_i \sim 1$, Thus, while infinite-*n* calculations can provide a useful qualitative guide, quantitative calculations of H-mode edge stability require studies with finite-*n* codes such as ELITE.

ELITE has also been employed in extensive studies of the edge stability of Quiescent H-Mode (QH) discharges on DIII-D. It has been found that QH mode discharges are typically marginally stable to current-driven peeling/kink modes in the edge. These QH-mode results are unlike those of Type-I ELMing discharges, which typically become unstable to peeling-ballooning or pure ballooning instabilities shortly before ELMs occur. A stability diagram based on perturbing around DIII-D discharge 115099 has been computed. The discharge is marginal to peeling instability at low-intermediate *n*, consistent with observations that ramping up the current results in large edge instability.

Observations of CIII light emission during ELMs on DIII-D have directly revealed the expected peeling-ballooning filamentary structure of ELMs (Fig. 3). Comparisons to the predicted linear mode structure have been made by calculating the unstable mode spectrum with ELITE just before the observed ELM, and comparing it against the CIII light emission. As shown in Fig. 4, the computed unstable mode spectrum reveals a filamentary structure similar to the observation. Non-linear simulations using BOUT also show strong similarities to both the predicted linear peeling-ballooning mode structure, as well as nonlinear simulation results.

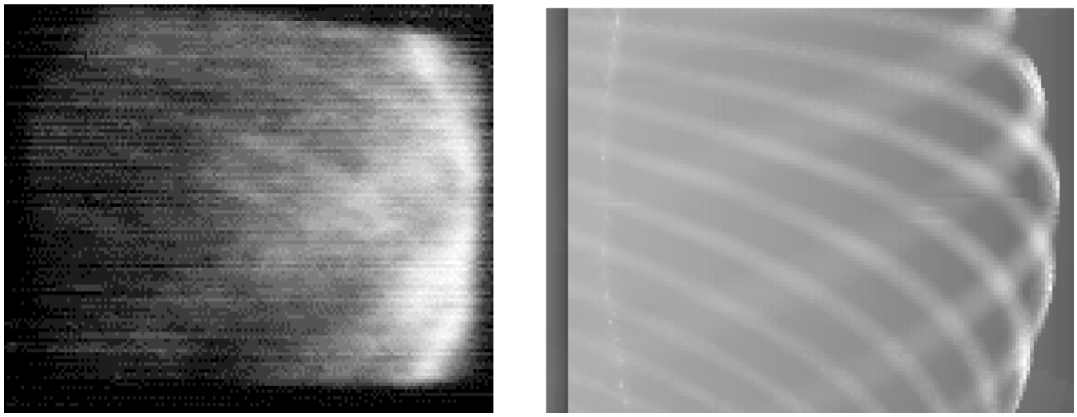

Fig. 4 CIII image during an ELM event in DIII-D discharge 119449 is compared to a plot of the mode structure predicted by ELITE for an n = 18 peeling-ballooning mode in an equilibrium reconstructed using measured profiles just prior to the ELM event.

The ELITE code has also been used to extensively explore the edge stability of a series of low-density discharges in which ELMs have been suppressed via resonant magnetic perturbations (RMP) driven by the I-coil on DIII-D. The stability analysis has clearly demonstrated that with RMP it is possible to hold the discharge in an H-mode steady state well below the instability threshold for ELMs (Fig 5). The peeling-ballooning stability of RMP discharges is in many ways similar to that of QH discharges. In both cases, due to low collisionality, the discharge is closer to the peeling stability boundary than to the peeling-ballooning or ballooning boundaries which are generally crossed during ELMs.

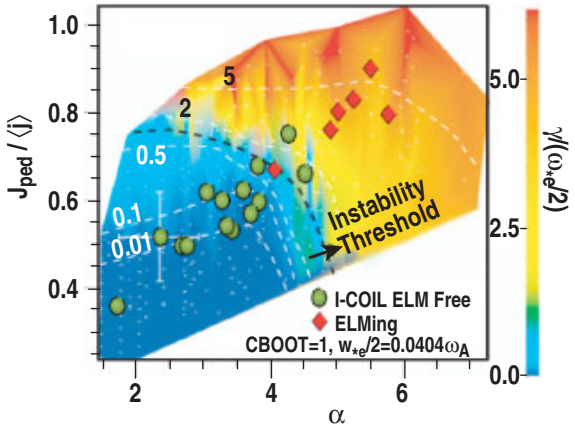

Fig. 5 A peeling-ballooning stability diagram calculated using ELITE for a series of I-Coil ELM-free and ELMing discharges of the same shape.

A study of the impact of the "squareness" of the discharge shape on edge stability has also been undertaken with ELITE. The results indicate that squareness can have a substantial impact on the pedestal stability bound. In particular, the pedestal stability bound at very high or very low squareness can be reduced up to a factor of two from the boundary at moderate, optimal squareness. Moving away from optimal squareness tends to reduce

access to second stability and moves the most unstable mode to higher *n*, consistent with DIII-D observations of smaller ELMs and lower pedestals at high squareness.

4.2. NONLINEAR ELM DYNAMICS

In collaboration with LLNL, we continue to conduct and analyze studies of ELM dynamics with the BOUT code, and further elucidate our proposal of two mechanisms to explain the full energy and particle losses during the ELM crash, which cannot be accounted for solely via loss of the filaments themselves: 1) The filaments, which remain connected at the ends to the hot core plasma, act as conduits, transporting heat and particles along the filament which is then lost onto open field lines via fast diffusion and/or secondary instabilities. 2) The growth and propagation of the modes strongly damps the sheared rotation in the edge region, collapsing the edge barrier and leading to a temporary return to enhanced L-mode transport. A number of nonlinear, electromagnetic BOUT simulations of ELMs in high density DIII-D discharges have been conducted, finding qualitative agreement with the observed filamentary structure of the early phase of the ELM, as well as radial propagation speed and poloidal extent.

Several new ELM simulations have also been carried out using the 3D MHD code NIMROD in an attempt to simulate late into the nonlinear regime with 22 toroidal harmonics. Linear runs using mode numbers 1, 6 and 21 as skeletal indicators of the growth rate spectrum were used to explore the (S,α) space with a series of equilibria. Stability boundaries were found and nonlinear runs in the vicinity of these are pending. Near-term efforts will focus on scanning increasing shear

4.3. RESISTIVE WALL MODE STABILITY

Modeling of feedback stabilization with the MARS-F stability code has yielded an improved understanding of RWM active stabilization experiments using the internal I-coils in DIII-D. The optimum phasing angle of the upper and the lower I-coils with respect to the sensor signal has been obtained and agrees with the experimentally measured angle. Moderate deviations from this phasing angle lead to a reduced feedback effectiveness. Large deviation of more than 90 degrees leads to a failure of the feedback, as expected from general theoretical expectations. This also correlates with the observation of disruptions in the experiments.

In collaboration with scientists at National Institute for Fusion Science in Japan (NIFS), a method has been formulated to compute the growth rate of a weakly unstable RWM in 3D configurations using results from ideal stability codes. It is shown that the RWM growth rate is approximately given by the rate at which the available free energy for the ideal external kink can be dissipated by the resistive wall. The eigenfunction is also approximately given by that of the external kink mode. This formulation is demonstrated by coupling the resistive wall calculations to the computation of the ideal MHD stability code

KSTEP that computes ideal stability of 3D toroidal systems approximately by transforming them into their 2D equivalent systems.

4.4. IDEAL STABILITY

The GATO ideal MHD stability code is now available as a worldwide computational service on FusionGrid (http://www.fusiongrid.org/). The new tools enable GATO to be conveniently run from a GUI interface with input and output linked to MDSplus in a secure environment. Presently, the service runs on a 2-CPU server. Data preparation and the invoking of a run are done through an IDL-based PreGATO utility. Both input and output data are written into MDSplus in a tree structure designed to be appropriate for any stability code. Future plans include adding a batch run feature and a run queue for efficient use of resources, and expanding the server to include more compute nodes.

A numerical GATO problem appeared at low aspect ratio and high toroidal mode number n in a benchmark among the three MHD stability codes MISHKA, GATO, and ELITE. An analysis showed the elliptic integrals used in the GATO vacuum calculations break down and that this was a general problem for most codes that employ a recursion relation to generate modified elliptic functions. A temporary solution was found by replacing the original Elliptic integral calculation by one with higher precision. This works remarkably well and allows calculation up to $n = 15$.

The packing algorithm in GATO was also significantly modified to be more flexible in turning off packing needed for strongly reversed cases where a large number of rational surfaces pile up in the core. This works extremely well for inverted q profiles and was critical to obtaining converged results in several recent DIII-D wall stabilized cases.

Lastly, the ideal stability property of configurations with a double transport barrier (DTB) was investigated using the GATO ideal stability code. This work extended a previous study of plasmas with an internal transport barrier (ITB), which suggested that β limit improves with increasing ITB width or moving the ITB location to the edge. The DTB stability calculations assumed a conducting wall at 1.5 times the minor plasma radius. Model equilibria for the study are computed using the TOQ code with a hyperbolic tangent pressure profile for both the ITB and edge transport barrier (ETB). By varying the ratio of ETB to ITB height with the location and width of the ETB fixed, the study suggests that modest ETBs can improve plasma stability. However, strong ETBs drive ideal MHD instabilities, and there is a window in the pedestal pressure, above which the ETBs drive instabilities with a substantial edge component.

4.5. DIII-D STABILITY ANALYSIS

Ideal stability analyses for several DIII-D discharges from the sawtooth and fully non-inductive experiments were completed. The sawtooth analysis results are consistent with the

ECE fluctuation measurements showing an ideal mode precursor prior to crash in the oval-shape discharge but no ideal mode in the bean-shape discharge. The stability analysis of several time-slices of a discharge from the fully non-inductive experiment suggests that the instability is driven strongly by the edge pressure gradient.

Equilibria with different q(0) for a DIII-D hybrid scenario discharge 117740 have also been analyzed for their 3/2 tearing mode structures. It was found that when q(0) approaches 1.0, the displacement of the 2/2 side-band dramatically increases in amplitude. This could give rise to anomalously large super-banana diffusion in the central region. As q(0) approaches sufficiently close to 1, the phase velocity of the 2/2 side-band becomes higher than the electron thermal speed. Under these conditions and for the observed parameters in DIII-D, enough negative current can be driven to account for the observed current deficit. This will prevent further drop in q(0) and avoid sawtooth.

5. ADVANCES IN RF HEATING AND FUELING RESEARCH

5.1. ICRF AND NBI FAST ION INTERACTIONS

The interaction between resonant plasma ion species and the fast Alfvén wave (FW) was investigated by coupling fast wave electric fields from the 2D full wave code TORIC4 to the Monte-Carlo code ORBIT-RF and compared to recent experimental measurements from Alcator C-Mod and DIII-D. An experimental C-Mod discharge with 5% hydrogen minority fundamental harmonic heating at 78 MHz and 1.0 MW RF power was used in the study. The wave field solutions from TORIC4 were approximated using a single dominant toroidal and poloidal wave number and input to ORBIT-RF. Results from the coupled ORBIT-RF and TORIC4 simulation agree well with the experimentally measured fast ion distribution from a CNPA diagnostic on C-Mod (Fig. 6). Compared to the linear absorption result obtained directly from TORIC4 with an assumed tail temperature of 20 keV, ORBIT-RF produces a much broader power deposition profile. The broadening is due to radial diffusion from the fast ion finite orbits and pitch angle scattering treated properly in ORBIT-RF.

ORBIT-RF has also been improved to generate random numbers from Gaussian probability distribution. The new ORBIT-RF was applied to study several DIII-D FW 60 MHz 4^{th} (#96043 and #122080), 5^{th} (#122993), and 116 MHz 8^{th} (#122087) harmonic discharges. ORBIT-RF simulations show strong wave-beam interactions under all 60 MHz experimental conditions and much weaker wave-particle interactions at 116 MHz, consistent with experimental observations. This is illustrated in Fig. 7. This may be explained by Coulomb scattering of finite-orbit resonant ions that curtails resonant interactions.

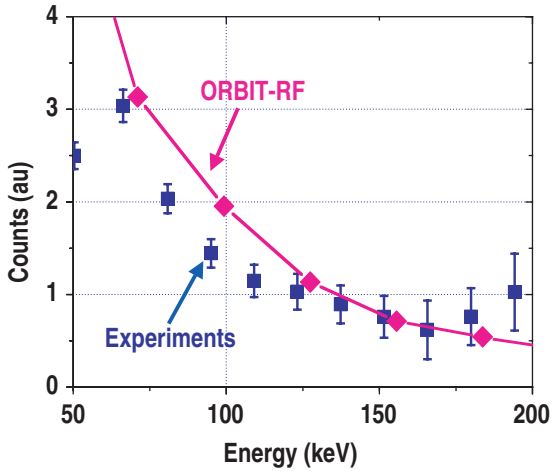

Fig. 6 Comparison of fast ion distribution from ORBIT-RF against the experimental measurement using a CPNA diagnostic for a C-Mod 78 MHz FW discharge.

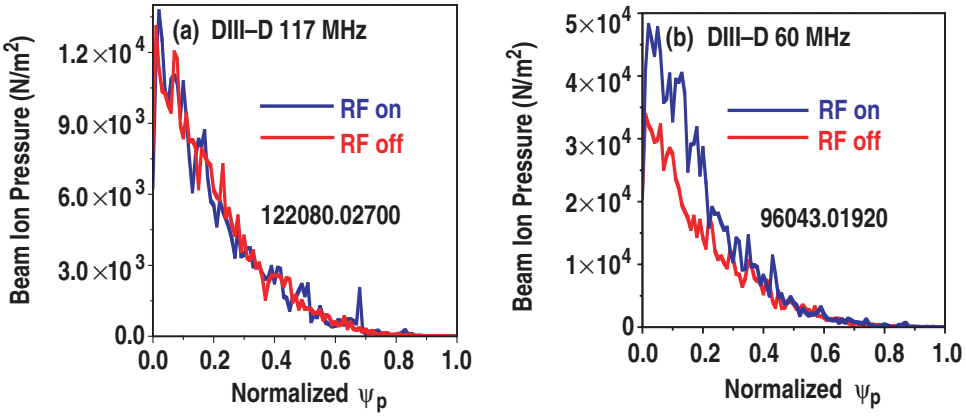

Fig. 7 Comparison of radial profiles of fast ion pressure from ORBIT-RF as a function of the normalized poloidal flux ψ_P for a DIII-D (a) 117 MHz and (b) 60 MHz FW discharge.

5.2. PELLET FUELING

The recently improved pellet ablation model that allows for effects of parallet flows, toroidicity, and arbitrary pellet poloidal entry angle was tested against DIII-D inside and outside launched pellet data. The modeling results generally agree with the experimental data. In the inside launched case, there is a deviation in the region $\rho/a > 0.85$. This is likely due to a large ELM triggered during the pellet injection event causing a large fraction of the edge pedestal density to be ejected from the plasma. This is also consistent with the modest discrepancy between the experimental and calculated particle fueling efficiencies, 46% versus 66%, respectively. For inside injection the triggered ELM is much less pronounced. Both measured and calculated fueling efficiencies are ~ 100%.

An incompressible fluid model for pellet breakup has shown that high velocity pellets are incompatible with the curved waveguides currently envisaged for ITER pellet fuelling. It is anticipated that in ITER, guide tubes will carry pellets of frozen DT accelerated by gas guns to a velocity of V~ 1 km/s to a launch position along the high-field-side of the separatrix surface. These tubes have one or more 90° bends. The new analysis predicts that the centrifugal force in the waveguide bends fractures pellets when V > 500 m/s. This is in agreement with recent ORNL experiments. For V > 1 km/s, successive fractures turn the pellet into a DT dust cloud. The fluid model finds that the cloud diameter decreases to preserve volume so that the dust cloud will extend along the guide tube. Interestingly, the pellet elongation is independent of pellet velocity. The pellet velocity limitations are avoided by pellet launch from the transformer core.

5.3. DISRUPTION MITIGATION USING MASSIVE GAS INJECTION

For disruption mitigation using massive gas injection, the rate of delivery of neutrals into the plasma must be sufficiently fast to prevent avalanche runaway growth. The propagation of a neutral gas and cold temperature front into the plasma has been calculated assuming poloidally and toroidally symmetric injection and by solving for the cooling front propagation velocity as an eigenvalue problem. Although the neutral penetration distance into the plasma is small, the radiation cooling of the plasma is exceedingly fast for high Z dense gases. Thus, the plasma can very quickly cool down to a temperature where the neutrals become transparent to the plasma. For ITER-like parameters and with a gas density at the boundary about 100 times the plasma density, the calculations indicate that the neutral gas penetration time is similar in magnitude to the time required to initiate the runaway current, and the avalanche runaway may be avoided.

A new "momentum model" has also been constructed to describe jet penetration in disruption mitigation experiments using massive gas injection from a collimated supersonic argon jet. In the DIII-D experiments, camera images indicate that the jets do not penetrate much past the separatrix. In the model, the jet forms a thin ionized boundary layer as it enters the plasma and the plasma and magnetic field are pushed aside. The net magnetic field inside is slightly less than outside the jet. The net magnetic force opposing the jet motion then balances the neutral pressure piling up as a shock behind the tip of the jet. Force balance yields an equation for the actual jet "tip speed" in terms of the "jet speed" in the absence of the shock. The jet cannot penetrate significantly unless the ratio of tip speed to jet speed, $U > U_{CRIT} = 1/4$, since otherwise the backward propagating shock wave reaches the rear surface. For DIII-D at B ~ 2 T, the model suggests that U is near U_{CRIT} so that penetration may be possible by lowering the field. A draft paper for submission to Phys. Rev. Lett. has been completed.

6. ADVANCES IN INNOVATIVE CONFINEMENT CONCEPT RESEARCH

6.1. 3-D EQUILIBRIUM RECONSTRUCTION

In collaboration with M. Zarnstorff of PPPL, a 3D filament code MFIT3D is being developed to reconstruct magnetic topology in stellarators and tokamaks with error or externally imposed toroidally asymmetric magnetic field. The plasma current distribution is modeled using toroidally asymmetric current filaments. MFIT3D is computationally inexpensive and capable of handling magnetic islands and stochasticity. This development is complementary to the ongoing collaboration with ORNL and Auburn University to build the V3FIT 3D reconstruction code that is based on VMEC and assumes nested flux surfaces.

6.2. MAGNETIC TARGET FUSION (MTF)

In collaboration with F. Thio, we have revised a draft paper on the MTF concept using converging gas jets to spherically implode magnetized plasma targets. The theory suggested that lowering the ratio of specific heats γ of the jets seems to promise the desired implosion intensity (target pressure and density) with lower and possibly more practical jet Mach numbers than calculated previously using $\gamma = 5/3$ for a mono-atomic plasma. At the moment this task is far from completed, because to realize the lower γ one needs to include effects of radiation and ionization in the form of a *second* outer plasma liner formed by some high-Z jet material such as argon. Borrowing from strong radiative shock theory, preliminary results suggest that with ionization and radiation, the effective adiabatic exponent could take values between 1.3 and 1.4 during the early phase of the implosion when ionization is significant, and manage to stay below 1.5 - 1.6 due to radiation at higher temperature.

7. Publications and Activity

7.1. PUBLICATIONS WITH PRIMARY THEORY AUTHORS

1. Brennan, D.P., S.E. Kruger, T.A. Gianakon, D. Schnack "A Categorization of Tearing Mode Onset in Tokamaks via Nonlinear Simulation," Nucl. Fusion **45**, 1178 (2005).
2. Candy, J. "Beta Scaling of Transport in Microturbulence Simulations," Phys. Plasmas **12,** 072307 (2005).
3. Choi, M., V.S. Chan, R.I. Pinsker, S.C. Chiu, W.W. Heidbrink "Monte-Carlo Orbit/Full Wave Simulation of Ion Cyclotron Resonance Frequency Wave Damping on Resonant Ions in Tokamaks" Phys. Plasmas **12**, 072505 (2005).
4. Chu, M.S., P.B. Parks, "Minimizing the MHD Potential Energy for the Current Hole Region in Tokamaks," Phys. Plasmas. **11,** 4859 (2004).
5. Chu, M.S., K. Ichiguchi "Effect of the Resistive Wall on the Growth Rate of Weakly Unstable External Kink Mode in General 3D Configurations," Nucl. Fusion **45**, 804 (2005).
6. Estrada-Mila, C., J. Candy, R.E. Waltz, "Gyrokinetic Simulations of Ion and Impurity Transport," Phys. Plasmas **12,** 022305 (2005).
7. Guo, S.C., M.S. Chu, "Study on Wall Locking of Multiple Tearing Modes in Reversed Field Pinch Plasmas," Phys. Plasmas **11,** 4050 (2004).
8. Ishizaki, R., P.B. Parks, N. Nakajima, M. Okamoto "Two-Dimensional Simulation of Pellet Ablation with Atomic Processes," Phys. Plasmas **11,** 4064 (2004).
9. Kinsey, J.E., R.E. Waltz, J. Candy "Nonlinear Gyro-kinetic Simulations of E×B Shear Quenching of Transport," Phys. Plasmas **12**, 062302 (2005).
10. Kinsey, J.E., F. Imbeau, G. Staebler, et al., "Transport Modeling and Gyrokinetic Analysis of Advanced High Performance Discharges," Nucl. Fusion **45**, 450 (2005).
11. Kinsey, J.E., G.M. Staebler, R.E. Waltz "Predicting Core and Edge Transport Barriers in Tokamaks Using the GLF23 Drift Wave Transport Model," Phys. Plasmas **12**, 052503 (2005).
12. Kinsey, J.E. "GLF23 Modeling of Turbulent Transport in DIII-D," Fusion Sci. Tech. **48**, 1060 (2005).
13. Lao, L.L., H.E. St. John, Q. Peng, J.R. Ferron, E.J. Strait, T.S. Taylor "MHD Reconstruction in the DIII-D Tokamak," Fusion Sci. Tech. **48**, 968 (2005).

14. Parks, P.B., L.R. Baylor "Effect of Parallel Flows and Toroidicity on Cross-Field Transport of Pellet Ablation Matter in Tokamak Plasmas," Phys. Rev. Lett. 94**,** 125002 (2005).
15. Parks, P.B., "A model of cusp magnetic field compression by an expanding plasma fireball," to appear in Phys. Plasmas Oct 2005.
16. Snyder, P.B., H.R. Wilson, and X.Q. Xu, "Nonlinear Dynamics of ELMs: Numerical Studies of Flow Shear Effects and 3D Nonlinear ELM Dynamics" Phys. Plasmas **12**, 056115 (2005).
17. Staebler, G.M., J.E. Kinsey, R.E. Waltz "Gyro-Landau Fluid Equations for Trapped and Passing Particles," to appear in Phys. Plasmas Oct 2005.
18. Turnbull, A.D., D.P. Brennan, M.S. Chu, L.L. Lao, P.B. Snyder, "Theory and Simulation Basis for Magnetohydrodynamic Stability in DIII-D," Fusion Sci. Tech. **48**, 875 (2005).
19. Waltz, R.E., J. Candy, F.L. Hinton, C. Estrada-Mila, J.E. Kinsey, "Advances in Comprehensive Gyro-kinetic Simulations of Transport in Tokamaks," Nucl. Fusion **45**, 741 (2005).
20. Waltz, R.E., J. Candy, "Heuristic theory of nonlocally broken gyro-Bohm scaling," Phys. Plasmas **12,** 072303 (2005).
21. Waltz, R.E. "ρ* scaling of physically realistic gyro-kinetic simulations of transport in DIII-D", Fusion Sci. Tech. **48**, 1051 (2005).
22. Wong, S.K., V.S. Chan, "A Drift-Kinetic Approach to Neoclassical Transport Theory for Plasma with Large Toroidal Rotation," Phys. Plasmas **11,** 4220 (2004).
23. Wong, S.K., V.S. Chan "The neoclassical Angular Momentum Flux in the Large Aspect Ratio Limit," Phys. Plasmas **12,** 092513 (2005).

7.2. ACTIVITY

- M.S. Chu visited NIFS for 3 months September 1 – November 30 to collaborate on RWM stability.
- D. Zhou from the Hefei Instituite of Plasma Physics completed his one-year tenure at General Atomics to collaborate on transport code and returned to China.
- Professor Y.Q. Liu from Chalmers University of Technology in Sweden visited GA for 1 month to collaborate on enhancement of the computational capability of the MARS-F/CHEASE package to study plasma stability and response physics.
- Professor S.J. Wang from the Hefei Institute of Plasma Physics in China visited GA for 3 months to collaborate on ideal MHD stability.
- R. Waltz visited CEA in Cadarache, France for two weeks (June 16-30) to collaborate with X. Garbet's group and gave a seminar on "Gyro-kinetic Simulations and Multi-scale Processes" and a tutorial on GYRO.

- C. Konz from IPP Garching visited GA for 3 months, and collaborated with P.B. Snyder on studies of edge localized mode stability with toroidal flow.
- Thomas Johnson from JET visited for three weeks to collaborate on benchmarking the ORBIT-RF code and preparing installation of the code for JET modeling.
- S. Murakami from Kyoto University visited for a week to benchmark ORBIT-RF against his GNET code. Additional issues for benchmarking have been identified.